Effect of parallel curtain walls on upward flame spread characteristics and mass loss rate over PMMA

Zunxin Zhao [a, b], Fei Tang [a, *], Lei Chen [b], Jianping Zhang [c], Jennifer Wen [d, *]

[a] State Key Laboratory of Fire Science, University of Science and Technology of China, Hefei, Anhui, 230026, China

[b] School of Automotive and Transportation Engineering, Hefei University of Technology, Hefei, Anhui 230009, China

[c] FireSERT, Belfast School of Architecture and the Built Environment, University of Ulster, Newtownabbey, BT37 0QB, United Kingdom

[d] Warwick fire, School of Engineering, University of Warwick, Coventry CV4 7AL, United Kingdom

Abstract

The effects of parallel curtain walls on the characteristics and mass loss rate of the upward flame spread over polymethyl methacrylate (PMMA) have been experimentally studied. The experimental research variables were the sample size and separation distance of the curtain wall. In the experimental setup, a PMMA plate was attached to one of the curtain walls. The results were analyzed to assess the effect of the curtain wall separation distance on the flame height. The special condition of two curtain walls with only a small distance between them was also analyzed. Analysis of experiments with systematically varied distances between the curtain walls has provided insight into factors such as air entrainment and the chimney effect. The results show the flame height evolution trend with the separation distance, and a new correlation to predict the global mass loss rate of the PMMA plate under the influence of parallel curtain walls, which can potentially be used in curtain wall design through optimization of the separation distance given fire safety requirements and practical needs.

Keywords: parallel curtain wall; upward flame spread; mass loss rate; PMMA

Graphical abstract

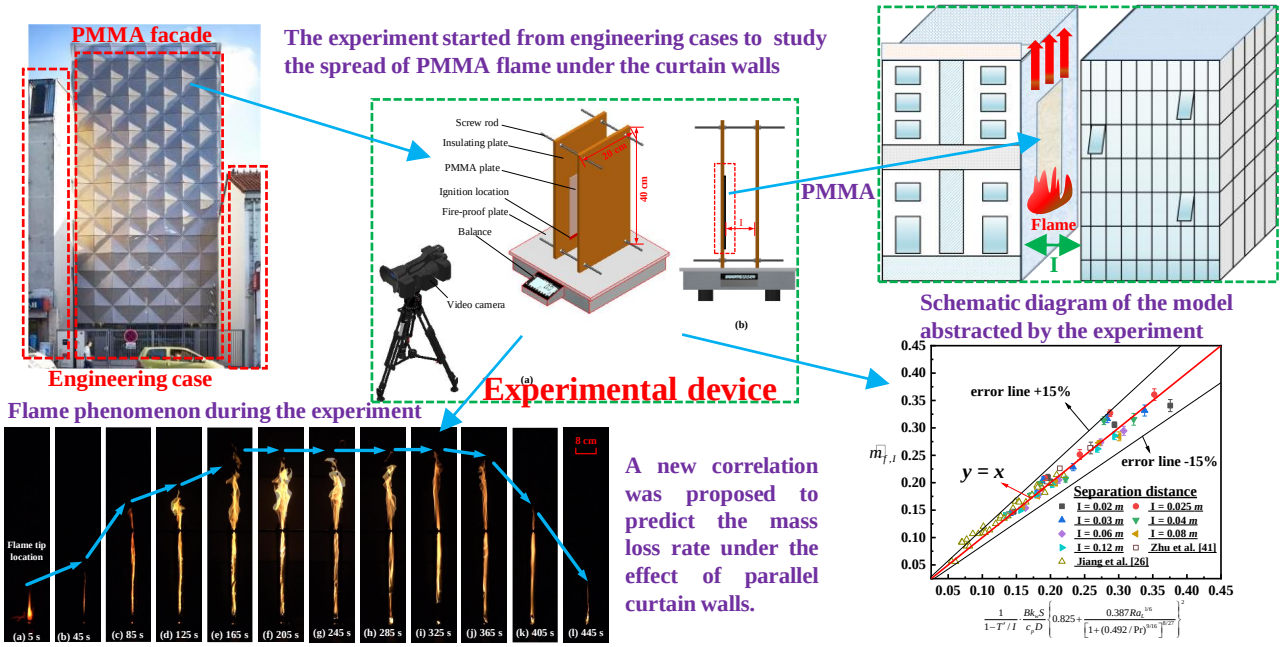

Nomenclature

B	mass transfer number	$\dot{m}_f$	mass loss rate *(g/s)*
c_p	specific heat of air $J/(g \cdot K)$	$\dot{m}_{f,I}$	mass loss rate with curtain wall separation distance of I (g/s)
D	hydraulic diameter *(m)*	$\dot{m}_{f,\infty}$	mass loss rate without curtain wall (g/s)
g	acceleration of gravity (m/s^2)	$\dot{m}_{total,I}$	total entrainment with curtain wall separation distance of I (g/s)
I	separation distance between installed parallel curtain wall and facade *(m)*	$\dot{m}_{total,\infty}$	total entrainment without curtain wall (g/s)
k_w	thermal conductivity of gas phase $W/(m \cdot K)$	$\dot{m}_{I',I}$	side entrainment with curtain wall separation distance of I (g/s)

K	global non-dimensional correction factor	$\dot{m}_{T',\infty}$	side entrainment for free boundary condition (g/s)
L	sample length *(m)*	$\dot{m}_{W,I}$	front entrainment with curtain wall separation distance of I (g/s)
$\dot{m}_{W,\infty}$	front entrainment for free boundary condition (g/s)	Greek symbols	
Pr	the Prandtl number	α	thermal diffusivity (m^2/s)
Ra_L	the Rayleigh number	β	thermal expansion coefficient
S	total surface area (m^2)	δ	entrainment strength
T'	sample thickness *(m)*	λ	relative strength difference between side entrainment and front entrainment
T_f	film temperature *(K)*	υ	kinematic viscosity, (m^2/s)
T_{flame}	flame temperature *(K)*	α_s	thermal diffusivity
$T_{pyrolysis}$	pyrolysis temperature *(K)*	τ	the characteristic time for solid sample to be exposed to the heat from the gas phase
T_∞	ambient temperature *(K)*		
W	sample width *(m)*		

1 Introduction

Decorative and insulation materials are installed in many industrial, office, and residential buildings. Fig. 1(a, b, c) shows the stadium for the 20th Olympic Games in Munich, Germany. The building was constructed in 1972 with a polymethyl methacrylate (PMMA) facade. In recent years, high-rise building fires have resulted in tighter regulations in many countries, banning the use of combustible facade systems. Following the Grenfell Tower fire, the British government banned combustible materials in buildings with stories over 18 m in height that contain a flat [1]. In China, the Ministry of Public Security requires that flammable and combustible materials are not used for exterior decoration on buildings greater than eight floors or 24 m in height [2]. However, for smaller buildings, combustible materials are still being used in many countries. Such materials include PMMA, extruded polystyrene (XPS), and polyurethane (PU) foam, which present considerable fire risk [3-6]. When these combustible solid materials burn, flames spread along the fuel surface [7, 8], and the flame propagation direction is influenced by the sample orientation. Vertical upward spread is the most dangerous flame propagation pattern; the flame and entrained air travel in the same direction as buoyancy, enhancing mixing and combustion.

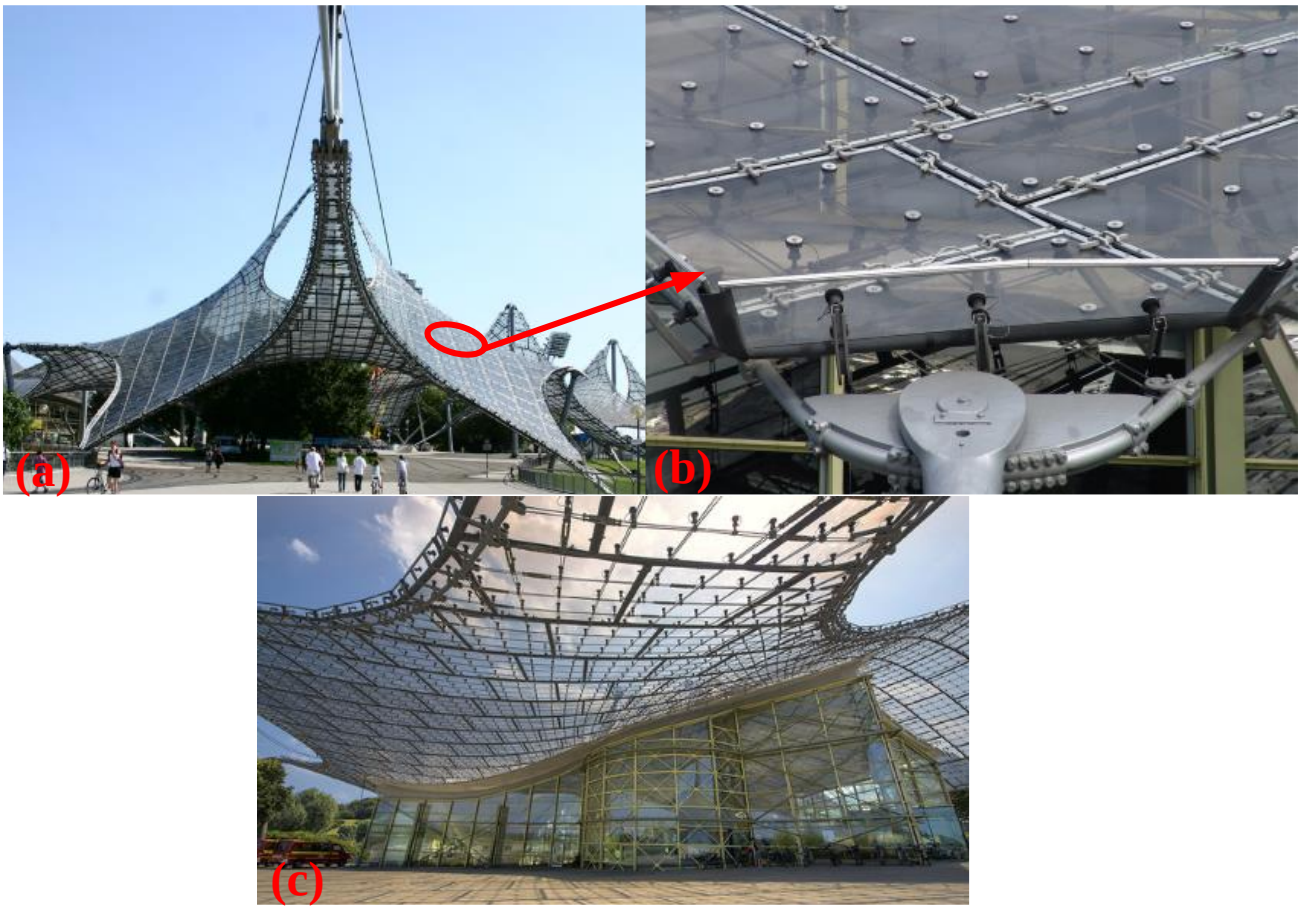

Fig. 1. Engineering application of PMMA material (reproduced from [9])

Previous investigations have addressed fire spread over different materials from different angles [10–15]. Studies have also been conducted on the burning characteristics of PMMA materials, providing useful information for this study [16–21].

Upward flame spread without curtain walls has been the subject of many investigations [22–27]. Rangwala et al. [24] conducted a theoretical analysis to predict lateral fuel diffusion during the initial stages of upward flame spread when the flame is laminar. Jiang et al. [25] experimentally studied the influence of the thickness and width of a PMMA sample on the upward flame propagation. Based on Emmons' hypothesis, they measured the flame spread rates and calculated the global mass loss. A relationship between the dimensionless flame height and the dimensionless heat release rate in the steady-state combustion process was proposed. Li et al. [26] investigated the upward flame spread over polyurethane (PU) foam with a concave structure. They found that the flame spread rate increased with time, and the mass loss rate increased with an increase in the ratio of the sidewall width to the facade

width. Hu et al. [28] studied the spread of flames on polyethylene wires with different inclination angles. The experiment compared the flame spread characteristics under different pressures.

Building facades are often accompanied by curtain walls, which are non-structural cladding systems for external building walls. Although curtain walls are generally made of non-combustible materials, they can alter flame spread behavior and potentially increase the fire hazard. To aid in development of fire detection and protection strategies for such buildings, insight into the upward flame spread over a combustible material in the presence of curtain walls is necessary. Some researchers have investigated the flame spread on curtain walls [29–32]. Wasan et al. [30, 31] conducted an experimental study and a numerical simulation to investigate the influence of the separation distance between the combustible slab and the curtain wall. The side wall in the experiment was 2.5 m high and 0.4 m wide, and the separation distances were 10.5 cm and 30.5 cm. It was found that with an increase in the separation distance, the flame spread rate decreased, and the flame temperature first decreased and then increased. This was contradicted by the numerical predictions of An et al. [32], who found that the flame spread rate first increased and then decreased with an increase in the separation distance. The side wall in their experiment was 1.8 m high and 0.5 m wide. The experimental separation distances were 4 cm, 6 cm, and 8 cm. The reason for this deviation may be that the test condition spacing designed by Wasan was relatively large, and the minimum spacing was already producing flame spread rate attenuation.

These studies highlighted that parallel curtain walls impact the flame spread by influencing the heat feedback and restricting air entrainment. However, further investigations are necessary to establish the influence trends and quantify the mass loss rate under different conditions, such as with varying separation distance and sample size. The purpose of this research is to experimentally study the effects of the separation distance between parallel curtain walls of different sizes and the building facade during upward flame spread. Parallel walls were represented by an insulating board, and PMMA was used for the building facade. Fifty-four sets of systematically designed experiments were

performed with six PMMA plate sizes ($20\times3\times0.2\,cm^3$, $20\times3\times0.5\,cm^3$, $20\times4.5\times0.2\,cm^3$, $20\times4.5\times0.5\,cm^3$, $20\times7.5\times0.2\,cm^3$, $20\times7.5\times0.5\,cm^3$) and nine separation distances (1 cm, 1.5 cm, 2 cm, 2.5 cm, 3 cm, 4 cm, 6 cm, 8 cm, and 12 cm). The flame spread characteristics and mass loss rate were recorded, and an analytical model based on air entrainment was developed to evaluate the global mass loss rate. This study provides valuable data for the validation of numerical models in future research.

2 Experiment

There are several types of PMMA materials, categorized according to processing technology, including casting, type, extrusion, and thermoforming types. PMMA material from casting has better thermo-physical properties and high transparency, and maintains its shape during pyrolysis and the counter-current fire spreading process. Casting-type PMMA was used in this study; its density is 1.18 g/cm^3.

Fig. 2(a, b) shows the experimental setup, including a PMMA plate, an insulating plate, a camera (Sony CX-900E), an igniter, and a load cell (Mettler Toledo load cell). The length of the PMMA plates was chosen as 20 cm as it was considered sufficiently long to observe the complete upward flame spread process in bench-scale tests; the PMMA plates were installed tightly on the left insulating plate. The insulating plates were made of a synthetic fireproof board with a width of 20 cm and a length of 40 cm. One insulating plate was used as a vertical facade on which the PMMA plates were fixed; the other was used as the curtain wall. The four corners of each insulating plate were punched with 10-mm holes. Between the two insulating plates, 9-mm diameter screw rods were passed through the punched holes and fixed with screws. Adjusting the screws changed the separation distance between the fireproof boards. In processing the fireproof plates and PMMA plates, 1 mm holes were punched on the centerline of the plates every 2 cm. For the experiment, the fireproof plate and the PMMA plate

were tied together with an iron wire to fix the PMMA plate. In studying the flame spread of solid materials, whether a material is thermally thin or thick can be determined by the thermal penetration depth of the material. For a thermally thin solid material with no internal temperature difference, the physical thickness d must be less than the thermal penetration depth ($d \langle\langle \sqrt{at} \approx \frac{k(T_s - T_0)}{\dot{q}''}$). From calculation, $d \langle\langle 5.19\, mm$. The minimum sample thickness in this experiment was 2 mm, and the maximum was 5 mm; the materials in this study were thermally thin solid materials. A steady burning stage was used to study the mass loss rate.

The separation distance between the PMMA and the curtain wall, represented by the insulating plate, was varied from 1–12 cm. All experimental samples were 20 cm in length. Two thicknesses were considered, 0.2 cm and 0.5 cm. For each thickness, three widths were used: 3 cm, 4.5 cm, and 7.5 cm. In the experiment, nine separation distances between the parallel curtain wall and the PMMA curtain wall were used: 1 cm, 1.5 cm, 2 cm, 2.5 cm, 3 cm, 4 cm, 6 cm, 8 cm, and 12 cm. A resistance wire with the same width as the PMMA plate was used as the igniter, and was fixed at the lower end of the sample. At the beginning of the experiment, the resistance wire was turned on to generate a high temperature to ignite the PMMA plate. After the sample was ignited, the power was turned off and the camera started recording. A video recorder (Sony CX-900E) was placed at the side to capture the flame structure details and the upward flame spread process. A fireproof board was placed between the load cell (with an accuracy of 0.01 g) and the test specimens to prevent heat damage to the load cell. The experiment was repeated three times for each set of test conditions to ensure the reliability of the experimental data; the average values of three tests were used for calculation.

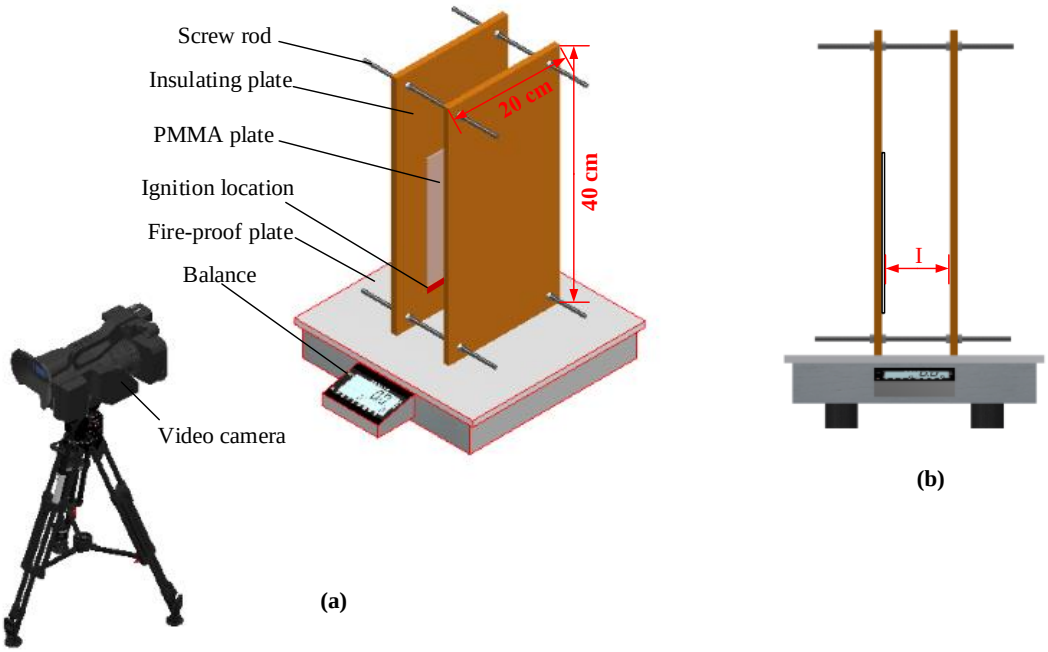

Fig. 2. Diagram of experimental setup

3 Results and discussion

3.1 Observation of PMMA upward flame spread

Fig. 3 shows a series of side-view images of the burning process from ignition to stable burning and extinction for a sample with dimensions of 200 mm × 30 mm × 5 mm and a separation distance of 2 cm. The starting time corresponds to the moment when the resistance wire power supply was turned off after igniting the PMMA plate. The PMMA plate with the low end close to the resistance wire was ignited in the initial stage, and the flame remained small with low illumination, as shown in Fig. 3 (Please also see the appendix, the experimental video of Fig. 3). The initial flame heated the unpyrolyzed region by radiation and convection to its pyrolysis temperature; the open flame ignited the pyrolysis gases. With further development of the combustion process, the flame quickly spread to the entire length of the PMMA plate; the combustion intensity increased with an increase in the amount of pyrolysis gas. In the presence of a parallel curtain wall, potential fire hazards associated with upward flame spread are magnified by the additional heat feedback from the curtain wall to the PMMA plate, resulting in an increased burning rate. The flame transitioned to bright yellow with increased soot production; the flame height quickly increased to its maximum. The combustion subsequently entered a steady stage, and the flame height remained almost constant. For a vertical plate, the critical Rayleigh number is 10^9.The Ra number for the entire combustion process ranged from 0–10^{10}; the flame gradually changed from laminar to turbulent. As shown in Fig. 3, during the initial stage, the flame was thin and close to the wall board, and burning was relatively slow and stable with no obvious flame fluctuations. With an increase in the burning area and flame radiation, the flame at the lower end of the PMMA remained relatively thin and stable in the laminar region; the flame at the upper end was turbulent, and expanded and thickened with a higher flame tip position. Fig. 4 shows the trend of the flame tip position over time for the selected test conditions. When the flame tip reached its highest position, the flame height remained almost constant for some time. In the later stage of the combustion

process, some burnout appeared at the bottom of the sample and the flame gradually moved upward. However, the flame burnout front moving upward was not obvious with the 30-mm-wide PMMA plate shown in Fig. 2. It was more obvious with the 7.5-cm-wide PMMA sample shown in Fig. 5, with dimensions of $20 \times 7.5 \times 0.5$ cm^3 and a separation distance of 3 cm, please also see the appendix, the experimental video of Fig. 5.

Fig. 6 shows the effect of the curtain wall separation distance on the steady-state flame spread (PMMA plate dimensions of $20 \times 3 \times 0.2$ cm^3). The flame height first increased then decreased, finally remaining steady with an increase in the separation distance. The increase in separation distance also reduced the air entrainment restriction of the curtain wall. The presence of parallel curtain walls induced the chimney effect, but restricted air entrainment; both effects alter the flame spread. When the separation distance was small, the dominant factor was the restriction on the front air entrainment, leading to a reduction in the oxygen supply, and a lower burning rate and flame height. Initially, with an increase in the separation distance, as shown in Fig. 6(b), the restriction on air entrainment decreased and the flame height increased. For relatively large separation distances, the chimney effect was found to dominate, with less restriction on air entrainment. However, as the separation distance was further increased, the chimney effect decreased, resulting in a reduction in the flame height. With a further increase in the separation distance, both factors became negligible, and the flame height remained nearly constant, the detailed experimental video of Fig. 6 can be found in the appendix.

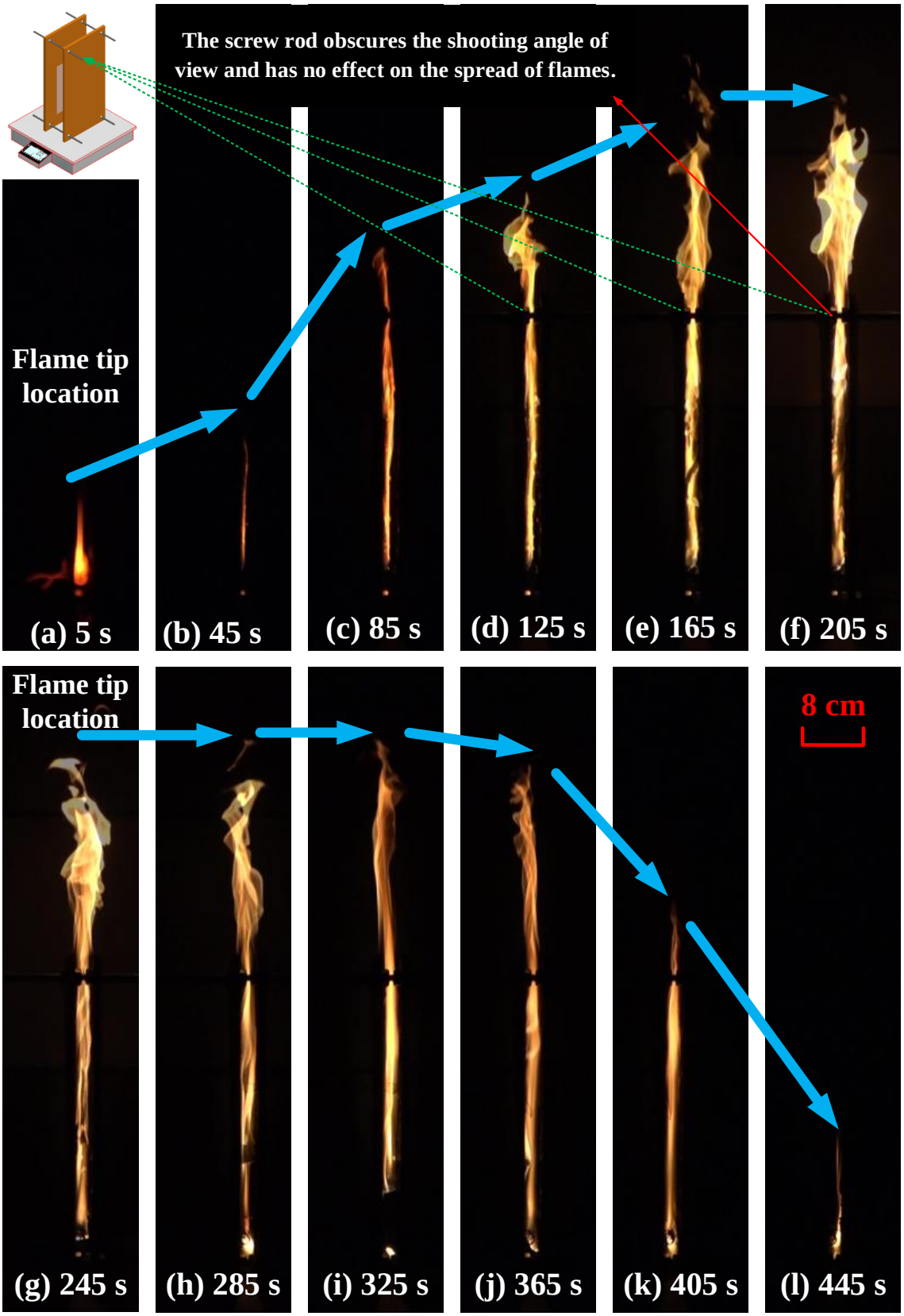

Fig. 3. Side view of upward flame spread at different times for 20 cm × 3 cm × 0.5 cm PMMA plate with 2 cm separation distance

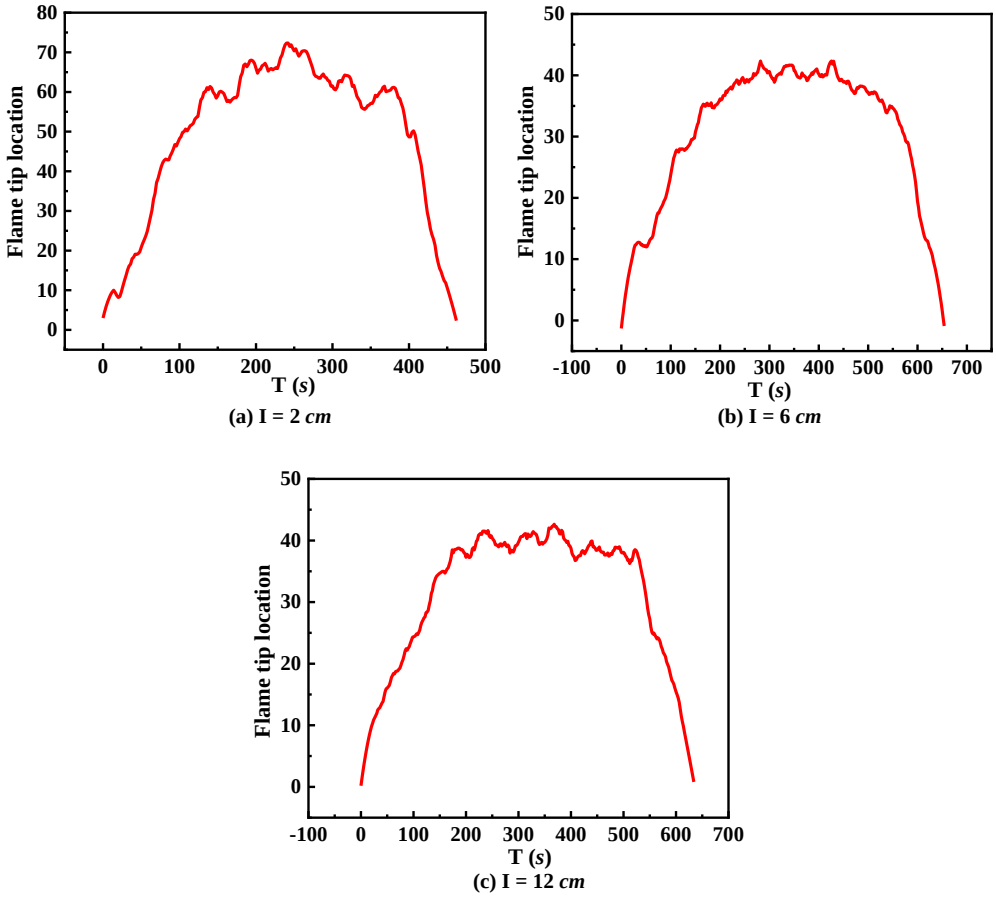

Fig. 4. Evolution of flame tip position over time ($L \times W \times T' = 20 \times 3 \times 0.5\, cm^3$).

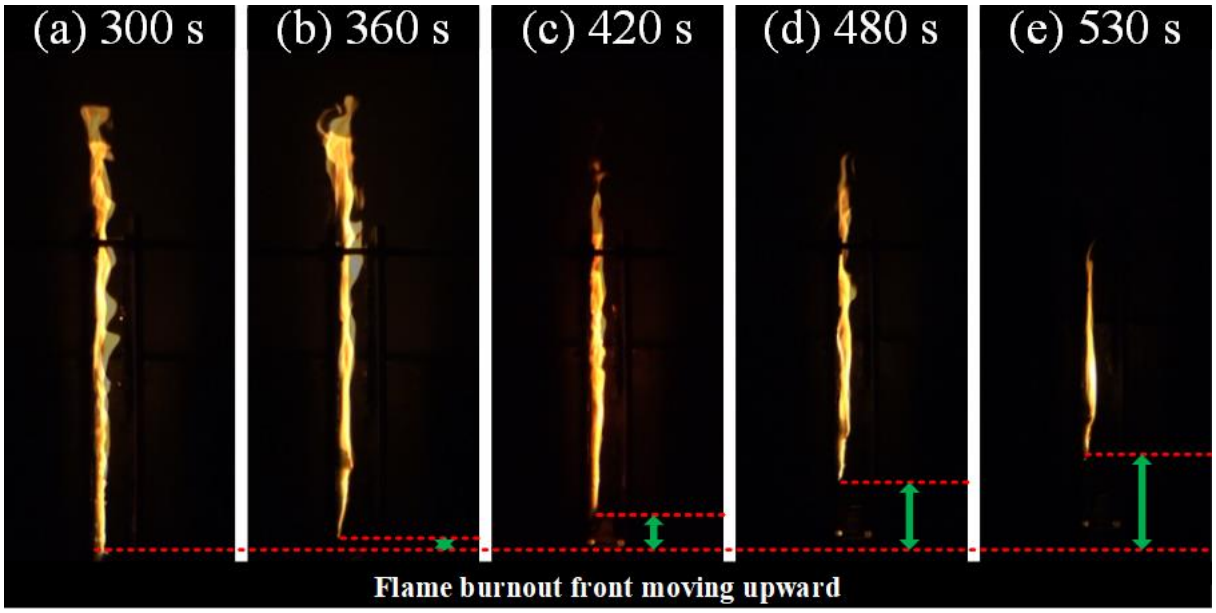

Fig. 5. Side view of flame burnout front moving upward at different times for 20 cm × 7.5 cm × 0.5 cm PMMA plate with 3 cm separation distance

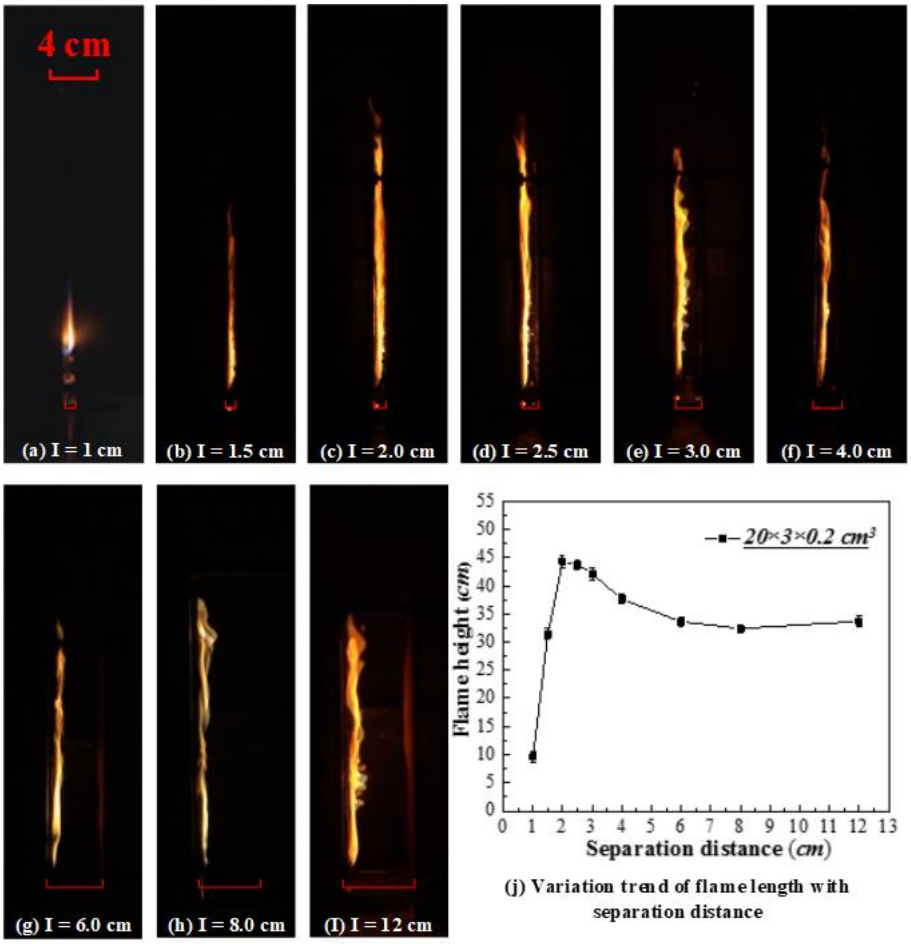

Fig. 6. Side view of upward flame spread under the influence of curtain wall for 20 × 3 × 0.2 cm^3 PMMA plate with different separation distances

3.2 Mass loss rate

Typical mass loss rate measurements for the entire combustion process are shown in Fig. 7. Three burning regions are observed: (i) from ignition to flame spread to the top of the PMMA plate; (ii) steady burning; (iii) the PMMA plate begins to fall. As shown in Fig. 8, the mass loss rate was calculated based on the measurements of the load cell. When the mass loss rate reached a quasi-steady state, the flame was considered to have reached the steady burning phase. The mass loss rates in regions (i) and (iii) change significantly with time owing to the transient burning behavior, whereas they remain almost constant in region (ii), as indicated by the red lines in Fig. 7; these values were chosen for comparison with measurements in different experimental conditions. The corresponding mass loss

rate for each experimental condition was calculated from the slope, as indicated by the red line in region (ii).

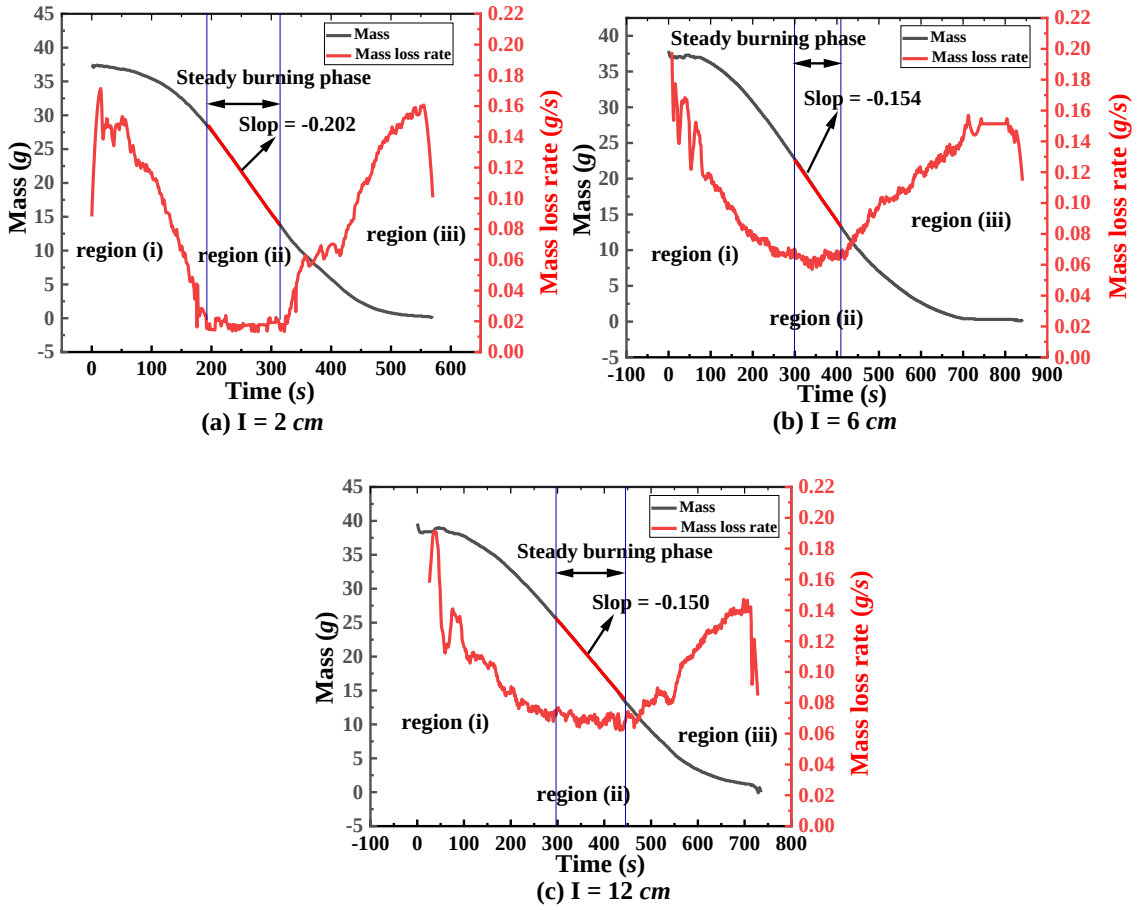

Fig. 7. Mass loss vs. time during upward flame spread following ignition for PMMA plate with

$$L \times W \times T' = 20 \times 3 \times 0.5\ cm^3$$

Fig. 8 compares the steady mass loss rate with different wall separation distances for six different PMMA sample dimensions. The mass loss rate increased with an increase in the sample width and thickness due to an increase in the sample surface area and the time to burnout. It first increased with the separation distance, then decreased before reaching a constant value for the three PMMA plate sizes. The maximum mass loss rate in most test conditions occurred with a separation distance of approximately 2 cm, which was consistent with the change in the observed flame height. The change trend of the mass loss rate with separation distance was also related to the restriction of air entrainment resulting from the curtain wall and the chimney effect. For separation distances less than 2 cm, the

restriction effect on the front air entrainment dominated; the mass loss rate increased with an increase in the separation distance. With a separation distance greater than 2 cm, there was ample oxygen for complete combustion of the pyrolysis gas, and air entrainment restriction had little effect on combustion. The chimney effect induced by the curtain wall was the dominant factor promoting combustion. A further increase in the separation distance (greater than 2 cm) weakened the chimney effect and decreased the mass loss rate. When the separation distance was sufficiently large, the effects of the curtain wall on air entrainment restriction and the chimney effect became negligible; the mass loss rate became constant, as shown in Fig. 8.

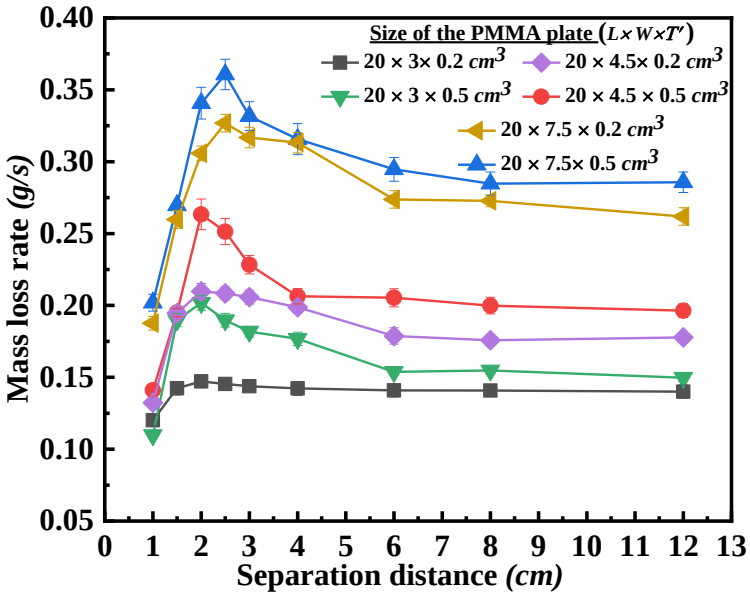

Fig. 8. Mass loss rate vs. curtain wall separation distance during upward flame spread for different PMMA sample dimensions

3.3 Modified mass loss rate formula

When the flame front reached the upper edge of the plate, the PMMA material at the igniter continued to burn, and there was no burnout region. This state can be reached in an actual PMMA wall fire after the flame spreads vertically upward and stabilizes. The burning area of the sample can be calculated as

$$S = W \cdot L + 2L \cdot T' \tag{1}$$

where S is the total surface area; W is the sample width; L is the sample length, and T' is the sample thickness.

For fire safety, the characteristic length transition is often used to quantify the dynamic fire behavior with irregular solid fuels. In this study, as the sample length is much larger than the sample width, the hydraulic diameter was used for the characteristic length calculation. The equivalent diameter method is commonly used to calculate characteristic length [33, 34]. The hydraulic diameter D can be calculated as

$$D = 2L(W + 2 \cdot T') / (L + W + 2 \cdot T') \tag{2}$$

Table 1. Physical properties used in mass loss rate calculation [25]

Physical properties used in mass loss rate calculation	
Mass transfer number (B)	1.32
Flame temperature (T_{flame})	1400 K
Pyrolysis temperature $(T_{pyrolysis})$	636 K
Specific heat of ambient gas phase (c_p)	$1.207\,kJ/(kg \cdot K)$
Thermal conductivity of gas phase (k_w)	$0.091\,W/(m \cdot K)$
Prandtl number (P_r)	0.703
Thermal diffusivity (α)	$168 \times 10^{-6}\,m^2/s$
Kinematic viscosity (υ)	$121 \times 10^{-6}\,m^2/s$

In Fig. 8, it is observed that the mass loss rate is almost constant in all test conditions when the separation distance between the curtain walls reaches 6 cm. These conditions are similar to a free boundary condition. Emmons [35] further extended the mass loss prediction based on the mass and heat transfer relation developed by Chilton–Colburn [36] and the hypothesis of Silver [37], which was extended from the Reynolds analogy. Jiang et al. [25] applied an upward plate convection

configuration from [38] over the entire range of Rayleigh numbers and expressed the global mass loss rate $\dot{m}_f$ for the entire pyrolysis area as

$$\dot{m}_f = \frac{Bk_w S}{c_p D}\left\{0.825 + \frac{0.387 Ra_L^{1/6}}{\left[1+(0.492/\mathrm{Pr})^{9/16}\right]^{8/27}}\right\}^2 \tag{3}$$

where c_p is the specific heat capacity of the air ($J/(g\cdot K)$); k_w is the thermal conductivity of the gas phase ($W/(m\cdot K)$); B represents the mass transfer number [25]; Pr is the Prandtl number. The calculation parameters are presented in Table 1. Ra_L is the Rayleigh number.

$$Ra_L = \frac{g\beta(T_f - T_\infty)D^3}{\upsilon\alpha} \tag{4}$$

where g is the acceleration due to gravity (m/s^2); T_f ($T_f = \left(T_{flame} + T_{pyrolysis}\right)/2$) and T_∞ are the film temperature [39] and ambient temperature, respectively (K); υ is the kinematic viscosity, (m^2/s); α is the thermal diffusivity of the air (m^2/s); β is the thermal expansion coefficient [40].

Using Eq. (3), the theoretical prediction of the global mass loss rate for the free boundary condition can be obtained. Compared with the measured mass loss rate data for all sample sizes at separation distances greater than 6 cm, they are in relatively good agreement, as shown in Fig. 9.

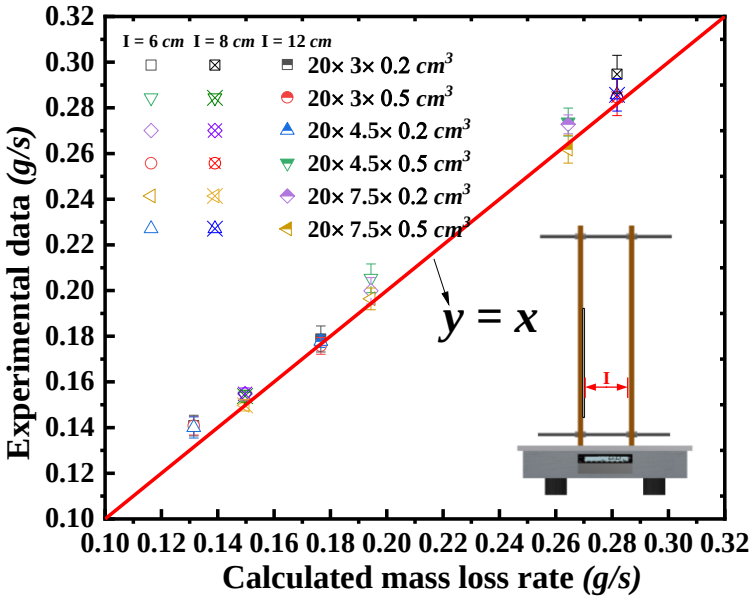

Fig. 9. Comparison of predicted and measured mass loss rates for separation

distances greater than 6 cm

To describe the effect of curtain walls on the decreasing tendency of the mass loss rate for separation distances from 2–6 cm, a global non-dimensional correction factor *K* is introduced for the mass loss rate:

$$K = \frac{\dot{m}_{f,I}}{\dot{m}_{f,\infty}} \tag{5}$$

where $\dot{m}_{f,I}$ is the mass loss rate with a curtain wall separation distance of I (g/s); $\dot{m}_{f,\infty}$ is the mass loss rate without a curtain wall or when the curtain wall separation distance is so large that its effect can be ignored (g/s). In this study, when $I \geq 6\,cm$, $K = 1$; when $I < 6\,cm$, K can be considered as a function of the sample width, thickness, and curtain wall separation distance.

$$K = fcn(W, T', I) \tag{6}$$

For free boundary conditions, the air entrainment due to the chimney effect includes entrainment from two sides of dimension T' and one front of dimension W, expressed as

$$\dot{m}_{total,\infty} = \dot{m}_{W,\infty} + 2\dot{m}_{T',\infty} \sim \delta(W + 2\lambda \cdot T') \tag{7}$$

where $\dot{m}_{total,\infty}$, $\dot{m}_{W,\infty}$, and $\dot{m}_{T',\infty}$ are the total air entrainment, and entrainment from the front and sides due to the chimney effect for the free boundary condition, respectively; λ is a coefficient describing the relative difference between air entrainment from the side direction and from the front direction. The effect of the curtain wall separation distance on the mass loss rate is introduced as $1-\frac{T'}{I}$. When the separation distance is sufficiently large (> 6 cm in this study), the effect of the curtain wall separation distance on the mass loss rate is negligible, and $1-\frac{T'}{I}$ approaches 1. As there is little effect from the side direction, the total air entrainment with a curtain wall separation distance of I is expressed as

$$\dot{m}_{total,I} = \dot{m}_{W,I} + 2\dot{m}_{T',I} \sim \delta\left[W(1-\frac{T'}{I}) + 2\lambda \cdot T'\right] \tag{8}$$

Thus, the non-dimensional correction factor *K* can be expressed as

$$K = \frac{\dot{m}_{f,I}}{\dot{m}_{f,\infty}} = \frac{\dot{m}_{total,\infty}}{\dot{m}_{total,I}} = \frac{W \cdot I + 2\lambda \cdot T' \cdot I}{W \cdot I - W \cdot T' + 2\lambda \cdot T' \cdot I} \quad (9)$$

The value of λ should be between 0 and 1. Fig. 10 compares the predicted $K \cdot \dot{m}_{f,\infty}$ and experimental data $\dot{m}_{f,I}$ for different values of λ; there is little difference with different values of λ. As the sample width is much greater than the thickness, air entrainment from the side is limited.

$$0 < \lambda < 1 \quad (10)$$

$$T' << W \quad (11)$$

$$2\lambda \cdot T' \cdot I << W \cdot I \quad (12)$$

From the analysis of Eqs. (10), (11), and (12), Eq. (13) is obtained as

$$K = \frac{\dot{m}_{f,I}}{\dot{m}_{f,\infty}} = \frac{\dot{m}_{total,\infty}}{\dot{m}_{total,I}} = \frac{W \cdot I}{W \cdot I - W \cdot T'} = \frac{(W \cdot I)/(W \cdot I)}{(W \cdot I - W \cdot T')/(W \cdot I)} = \frac{1}{1 - T'/I} \quad (13)$$

Considering only the effect from the sample front, the non-dimensional factor *K* becomes

$$K = \frac{\dot{m}_{f,I}}{\dot{m}_{f,\infty}} = \frac{\dot{m}_{W,\infty}}{\dot{m}_{W,I}} = \frac{1}{1 - T'/I} \quad (14)$$

Combining Eq. (3) and Eq. (14), the mass loss rate with curtain wall constraints and different separation distances can be characterized as

$$\dot{m}_{f,I} = K \cdot \dot{m}_{f,\infty} = \frac{1}{1 - T'/I} \cdot \frac{B \cdot k_w \cdot S}{c_p \cdot D} \left\{ 0.825 + \frac{0.387 Ra_L^{1/6}}{\left[1 + (0.492/\mathrm{Pr})^{9/16} \right]^{8/27}} \right\}^2 \quad (15)$$

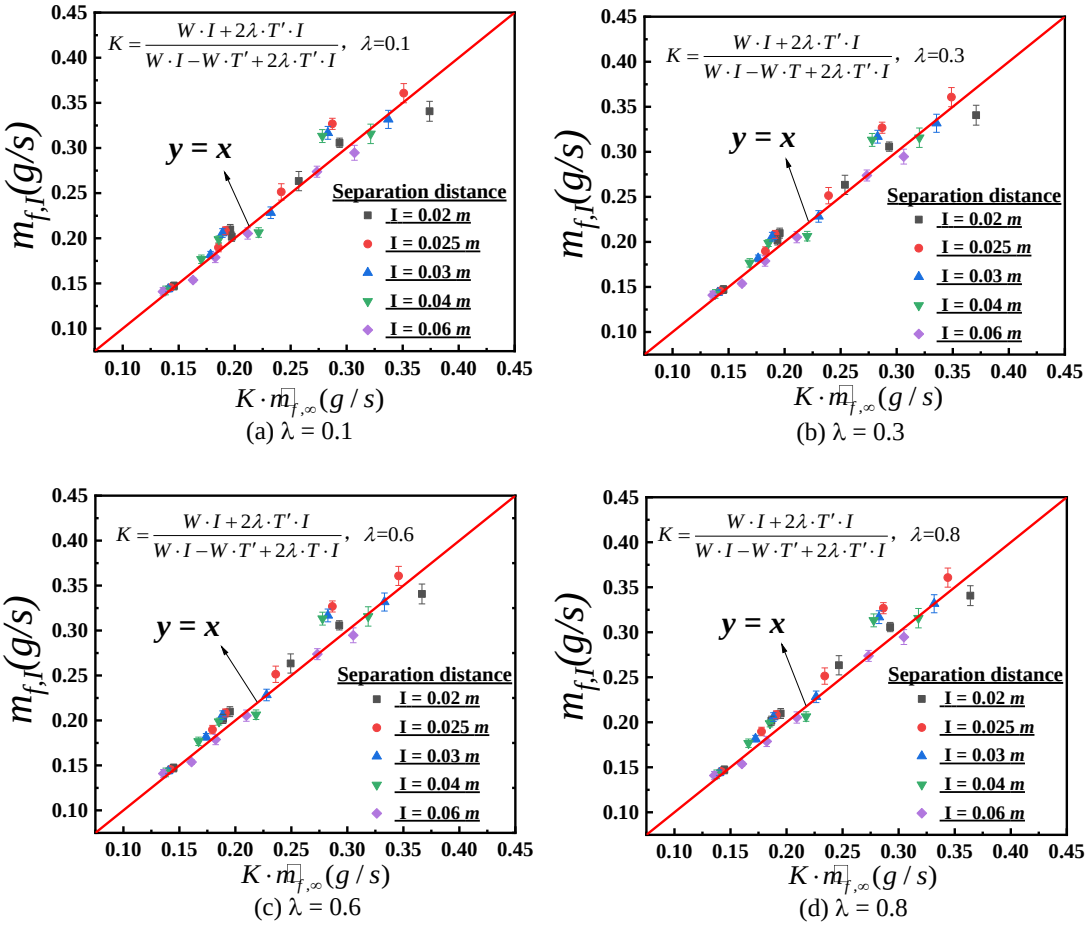

Fig. 10. Comparison of predicted and measured mass loss rates corrected by non-dimensional factor K with different constant values of λ

Fig. 11 compares the predicted mass loss rate using Eq. (15) and the non-dimensional factor K without considering side entrainment, with the current experimental data for separation distances from 2–12 cm and data reported by Jiang et al. [25] and Zhu et al. [41]. As shown in Fig. 11, the predictions are similar to the experimental measurements. Zhu et al. [41] studied the effect of the separation distance between the wall and a thermally thin PMMA plate on the upward flame spread. Unlike the setup in this study, in their tests, thin PMMA plates were placed in hollowed-out metal plates. Air could be entrained in all directions and there was no restriction on the entrainment. Both sides of the PMMA plate could be ignited, and the burning area was larger than in this study, in which PMMA plates were installed tightly only on the left insulating plate. The relatively good agreement between the predictions and measurements indicates that Eq. (15) is suitable for predicting the mass loss rate

of upward flame spread. Although derived from measurements under the influence of a curtain wall, it is also applicable to previous tests without parallel curtain walls [25]. In such tests, the separation distance tends to infinity ($K = 1$).

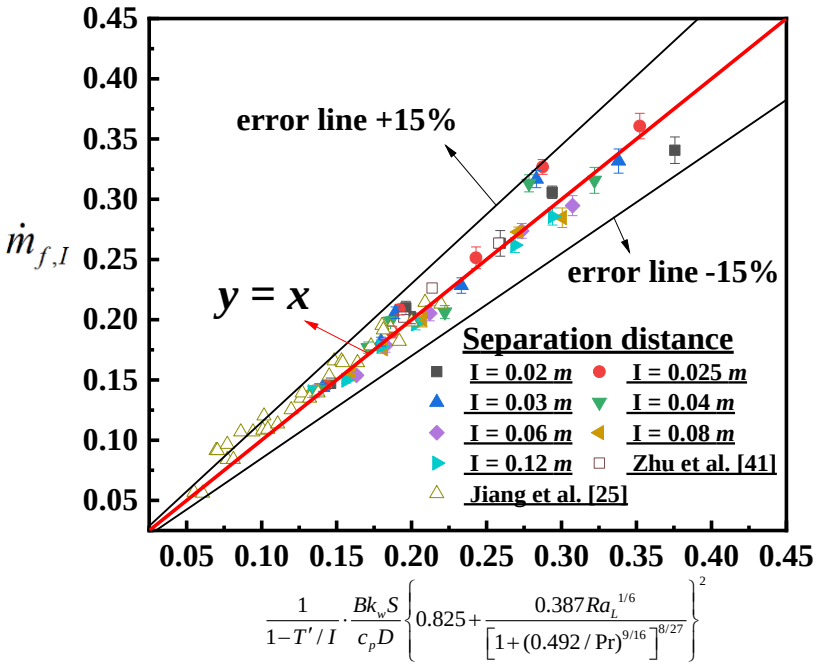

Fig. 11. Comparison of predicted mass loss rate using Eq. (15) with experimental measurements without considering side effect, and previous studies without parallel curtain walls

4 Conclusions

In this study, the effects of curtain walls on the characteristics of upward flame spread over a PMMA plate were investigated experimentally. The major findings are presented as follows:

(1) With an increase in the curtain wall separation distance, the flame height first increases and then decreases before reaching a stable value.

(2) A correlation was derived to predict the mass loss rate based on the formula proposed by Jiang et al. (2018), with modifications to quantify the decrease in the mass loss rate with an increase in the curtain wall separation distance.

Further experimental and Computational Fluid Dynamics (CFD) studies should be conducted to verify that the derived correlation is suitable for predicting the mass loss rate for upward flame spread over PMMA plates with and without curtain walls. Without curtain walls, the separation distance in the correlation should be set to infinity. The correlation should be useful in actual design for balancing fire safety requirements and the separation distance between the PMMA and curtain wall.

Acknowledgements

This work was supported by the National Nature Science Founds of China (Grant Nos. 52076066 and 51776060), and SAFEA: High-End Foreign Experts Project.

References

1. Ministry of Housing, Communities and Local Government. Final Impact Assessment: Ban on combustible materials in external wall systems. Building (Amendment) Regulations 2018 SI 2018/1230.
2. National standards of People's Republic of China (GB50016-2014), Code for fire protection design of high-rise civil buildings. Ministry of Public Security of the People's Republic of China.
3. An WG, Jiang L, Sun JH, Liew KM (2015) Correlation analysis of sample thickness, heat flux, and cone calorimetry test data of polystyrene foam. J. Therm. Anal. Calorim.119: 229-238.
4. An WG, Sun JH, Liew KM, Zhu GQ (2017) Effects of building concave structure on flame spread over extruded polystyrene thermal insulation material. Appl. Therm. Eng. 121: 802-809.
5. An WG, Li S, Yin XW, Peng LJ. (2021) Combustion and fire safety of energy conservation materials in building vertical channel: Effects of structure factor and coverage rate. Case Stud. Therm. Eng. 24: 100847.
6. An WG, Yin XW, Cai ML, Gao YJ, Wang HT. (2019) Influence of vertical channel on downward flame spread over extruded polystyrene foam. Int. J. Therm. Sci. 145: 105991.
7. Gollner MJ, Huang XY, Cobian J, Rangwala AS, Williams FA (2013) Experimental study of upward flame spread of an inclined fuel surface. P. Combust. Inst. 34: 2531-2538.
8. Zhang Y, Ji J, Wang QS, Huang XJ, Wang QH, Sun JH (2012) Prediction of the critical condition for flame acceleration over wood surface with different sample orientations. Combust. Flame159 (9):2999-3002.
9. Fig. 1(a, b) reproduced from http://www.bml365.com/show/case/detail/148; Fig. 1(c) reproduced from https://www.sohu.com/a/25166952_185885
10. Carmignani L, Rhoades B, Bhattacharjee S (2018) Correlation of Burning Rate with Spread Rate for Downward Flame Spread Over PMMA. Fire Technol. 54(3):1-12.
11. Gao Y, Zhu G, Zhu H, An W, Yu M, Huang J, Xia Y (2018) Experimental Analysis of Critical Acceleration Condition for Two-Sided Upward Flame Spread Over Inclined Thin Fuel Surfaces. Fire Technol. 55(3):755-771.
12. Zhao K, Gollner MJ, Liu Q, Gong J, Yang L (2020) Lateral flame spread over PMMA under forced air flow. Fire Technol. 56: 801-820.
13. Gou FH, Xiao HH, Jiang L, Li M, Zhang MM, Sun JH (2020) Upward flame spread over an array of discrete thermally-thin PMMA plates. Fire Technol. https://doi.org/10.1007/s10694-020-01068-9.
14. Huang XY, Gao J (2020) A review of near-limit opposed fire spread. Fire Saf. J. 103141.

15. Zhu N, Huang XY, Fang J, Yang LZ, Hu LH. (2021) Transitional flame-spread and fuel-regression behaviors under the change of concurrent wind. Fire Saf. J. 120(2):103015.
16. Zhu H, Gao YJ, Pan RL, Zhong B (2019) Spacing effects on downward flame spread over thin PMMA slabs. Case Stud. Therm. Eng. 13: 100370.
17. Ranga R H R, Korobeinichev O P, Raghavan V, Tereshchenko A G, Trubachev S A, Shmakov A G (2019) A study of the effects of ullage during the burning of horizontal PMMA and PMMA surfaces. Fire Mater. 43(3): 241-255.
18. Ranga R H R, Korobeinichev O P, Harish A, Raghavan V, Kumar A, Gerasimov I E, Gonchikzhapov M B, Tereshchenko A G, Trubachev S A, Shmakov A G (2018) Investigation of the structure and spread rate of flames over PMMA slabs. Appl. Therm. Eng.130: 477-491.
19. Singh A V, Gollner M J (2017) Steady and transient pyrolysis of a non-charring solid fuel under forced flow. Proc. Combust Inst. 36: 3157-3165.
20. Miller C H, Gollner M J (2015) Upward flame spread over discrete fuels. Fire Saf. J. 77: 36-45.
21. Ma YX, Hu LH, Huang YJ, Zhu N, Fujita O (2021) Effect of sample thickness on concurrent steady spread behavior of floor and ceiling flames. Combust. Flame 233: 111600.
22. Pizzo Y, Consalvi JL, Querre P, Coutin M, Audouin L, Porterie B (2008) Experimental observations on the steady-state burning rate of a vertically oriented PMMA slab. Combust. Flame 152: 451-460
23. Leventon IT, Stoliarov SI (2013) Evolution of flame to surface heat flux during upward flame spread on poly (methyl methacrylate). P. Combust. Inst. 34: 2523-2530.
24. Rangwala AS, Buckley SG, Torero JL (2007) Upward flame spread on a vertically oriented fuel surface: the effect of finite width. P. Combust. Inst. 31 (2): 2607-2615.
25. Jiang L, He JJ, Sun JH (2018) Sample width and thickness effects on upward flame spread over PMMA surface. J. Hazard. Mater. 342: 114-120.
26. Li JT, Yan WG, Zhu HY, Wang QS, Sun JH (2012) Experimental study on the fire spread in high-rise buildings with U-shaped outside-facade structure. Fire safety science 21(4):167-173.
27. Tsai KC (2011) Influence of sidewalls on width effects of upward flame spread. Fire Saf. J. 46: 294-304.
28. Hu LH, Zhang YS, Yoshioka K, Izumo H, Fujita O (2015) Flame spread over electric wire with high thermal conductivity metal core at different inclinations. P. Combust. Inst. 35(3):2607-2614.

29. Ma X, Tu R, An WG, Xu L, Luo SF, Wang JW, Tang F (2020) Experimental study of interlayer effect induced by building facade curtain wall on downward flame spread behavior of polyurethane. Appl. Therm. Eng. 167: 114694.
30. Wasan SR, Van Hees P, Merci B (2011) Study of pyrolysis and upward flame spread on charring materials-Part I: experimental study. Fire Mater. 35: 209-229.
31. Wasan SR, Rauwoens P, Vierendeels J, Merci B (2011) Study of vertical upward flame spread on charring materials-Part II: numerical simulations. Fire Mater.35: 261-273.
32. An JT, Jiang Y, Qiu R, Wang Y (2012) Numerical study of polyurethane foam fire between narrow vertical parallel walls. J. Saf. Sci. Technol. 8: 5-9.
33. Hu LH, Tang F, Wang Q, Qiu ZW (2013) Burning characteristics of conduction-controlled rectangular hydrocarbon pool fires in a reduced pressure atmosphere at high altitude in Tibet. Fuel 111: 298-304.
34. Tu R, Fang J., Zhang YM, Zhang J, Zeng Y (2013) Effects of low air pressure on radiation-controlled rectangular ethanol and n-heptane pool fires. P. Combust. Inst. 34 (2): 2591-2598.
35. Emmons HW (1956) The film combustion of liquid fuel. J. Appl. Math. Mech. Z. Angew. Math. Mech. 36 (1-2):60-71.
36. Chilton TH, Colburn AP (1934) Mass transfer (absorption) coefficients prediction from data on heat transfer and fluid friction. Ind. Eng. Chem. Res. 26 (11): 1183-1187.
37. Silver S (1950) Application of the Reynolds analogy to combustion of solid fuels. Nature 165 (4201): 725-726.
38. Bergman TL, Incropera FP (2011) Fundamentals of Heat and Mass Transfer, John Wiley & Sons.
39. Jiang L, Miller CH, Gollner MJ, Sun JH (2017) Sample width and thickness effects on horizontal flame spread over a thin PMMA surface, P. Combust. Inst. 36 (2): 2987-2994.
40. Richard T, Long J, Jose T, Quintiere J (2000) Scale and Transport Considerations on Piloted Ignition of PMMA. Fire Safety Science-Proceedngs of the 6th International Symposium 6: 567-578.
41. Zhu H, Zhu GQ, Gao YJ (2017) Experimental Studies on the Effects of Spacing on Upward Flame Spread over Thin PMMA. Fire Technol. 53 (2): 673-693.